Solid State Phenomena Vol. 150 (2009) pp 73-100
online at http://www.scientific.net

Online available since 2009/Jan/13

Statistical Thermodynamics and Surface Phase Transitions of Interacting Particles Adsorbed on One-Dimensional Channels Arranged in a Triangular Cross-Sectional Structure

P.M. Pasinetti[1,a], F. Romá,[1,2,b], J.L. Riccardo[1,c] and A.J. Ramirez-Pastor[1,d]

[1]Departamento de Física, Instituto de Física Aplicada, Universidad Nacional de San Luis-CONICET, Chacabuco 917, 5700, San Luis, Argentina

[2]Centro Atómico Bariloche, Av. Bustillo 9500, 8400, S. C. de Bariloche, Argentina

[a]mpasi@unsl.edu.ar, [b]froma@unsl.edu.ar, [c]jlr@unsl.edu.ar, [d]antorami@unsl.edu.ar

Keywords: Lattice-gas models, adsorption thermodynamics, surface phase transitions, Monte Carlo simulations.

Abstract. Monte Carlo simulations and finite-size scaling analysis have been carried out to study the critical behavior in a submonolayer lattice-gas, which mimics a nanoporous environment. In this model, one-dimensional chains of atoms were arranged in a triangular cross-sectional structure. Two kinds of lateral interaction energies have been considered: (1) w_L, interaction energy between nearest-neighbor particles adsorbed along a single channel and (2) w_T, interaction energy between particles adsorbed across nearest-neighbor channels. We focus on the case of repulsive transverse interactions ($w_T > 0$), where a rich variety of structural orderings are observed in the adlayer, depending on the value of the parameters k_BT/w_T (k_B being the Boltzmann constant) and w_L/w_T. For $w_L/w_T = 0$, successive planes are uncorrelated, the system is equivalent to the triangular lattice, and the well-known $(\sqrt{3}\times\sqrt{3})$ $[(\sqrt{3}\times\sqrt{3})^*]$ ordered phase is found at low temperatures and a coverage, θ, of 1/3 [2/3]. In the more general case ($w_L/w_T \neq 0$), the competition between interactions along a single channel and the transverse coupling between sites in neighboring channels leads to a three-dimensional adsorbed layer. Consequently, the $(\sqrt{3}\times\sqrt{3})$ and $(\sqrt{3}\times\sqrt{3})^*$ structures "propagate" along the channels and new ordered phases appear in the adlayer. The influence of each ordered phase on adsorption isotherms, differential heat of adsorption and configurational entropy of the adlayer has been analyzed and discussed in the context of the lattice-gas theory. Finally, the Monte Carlo technique was combined with the recently reported free energy minimization criterion approach (FEMCA) [F. Romá et al.: Phys. Rev. B Vol. 68 (2003), art. no. 205407] to predict the critical temperatures of the surface-phase transformations occurring in the adsorbate. The excellent qualitative agreement between simulated data and FEMCA results allows us to interpret the physical meaning of the mechanisms underlying the observed transitions.

Introduction

Lattice-gas models have been extensively investigated in the last decades because they provide a theoretical framework for the description of many physical, chemical, and biological systems. The adsorption thermodynamics and the understanding of surface phenomena have been greatly benefited from the development of these models [1,2]. In this sense, the more recognized examples are the Langmuir adsorption model [1,3] and the Ising model of magnetism [4-7]. More recently, a number of contributions have been devoted to the study of adsorption of gases on solid surfaces [8-21]. These papers have included the effects of lateral interactions [8-12], surface heterogeneity [13], multisite occupation [10,14-21], etc. Among them, Phares et al. [10] have studied the structural orderings occurring in a wide variety of experimental and theoretical systems and its influence on the corresponding phase diagrams.

Recently, the advent of modern techniques for building single and multiwalled carbon nanotubes [22-26] has considerably encouraged the investigation of the gas-solid interaction (adsorption and

transport of simple and polyatomic adsorbates) in such low-dimensional confining adsorption potentials. The design of carbon tubules, as well as of synthetic zeolites and aluminophosphates such as AlPO4−5 (Refs. [27,28]) having narrow channels, literally provides a way to the experimental realization of quasi-one-dimensional adsorbents. Many studies on conductivity, electronic structure, mechanical strength, etc., of carbon nanotubes are being currently carried out. However, the amount of theoretical and experimental works done on the interaction and thermodynamics of simple gases adsorbed in nanotubes is still limited.

A problem of considerable importance in adsorption is that of determining where on the nanotube bundles the gas molecules adsorb [29-43]. Theoretically there are three possible groups of adsorption sites on bundles of close-ended singlewalled carbon nanotubes: (1) interstitial channels formed between the tubes, (2) grooves formed between two adjacent tubes on the bundle surfaces, and (3) exterior surface of individual tubes [30]. For open-ended tubes, a fourth group of adsorption sites can be identified in the interior of individual tubes [30]. Access to each group of adsorption sites is determined by the size of the adsorbate, the size of the nanotubes forming the bundles, the degree of homogeneity of the bundles, and the presence or absence of chemical compounds blocking access to the sites [30,43-45].

Numerous experimental and theoretical studies of gas adsorption on nanotube bundles suggest that the admolecules form one-dimensional (1D) systems or lines when adsorb within interstitial channels [35,36] inside nanotubes [36-38] or along the groove sites [39-41]. For theoretical purposes, adsorption in these lines can be treated in the one-dimensional lattice-gas approach [11,18]. This is, of course, an approximation to the state of real adsorbata in nanotubes, which is justified because thermodynamics and transport coefficient can be analytically resolved in these conditions. An example of this kind of models is presented in Refs. [37] and [38]. The authors proposed a simple model for adsorption inside a nanotube. That is a lattice-gas model with two kinds of sites. One was a one-dimensional line of sites, which the authors called axial sites, surrounded by a set of cylindrical shell sites. By using mean-field theoretical approach [37] and Monte Carlo (MC) simulations [38], a rich phase behavior was obtained for attractive or repulsive character of the interspecies interaction.

The influence of transverse interactions between adjacent lines was also studied in the case of adsorption in interstitial channels [46]. In Ref. [46], Cole *et al.* presented a localized anisotropic lattice-gas model with lateral interactions between neighboring atoms within the same channel and attractive transverse interaction between neighbor interstitial channels (arranged in a honeycomb lattice). While the strictly 1D system does not exhibit critical behavior, a phase transition occurs in the system with interacting channels. This phase transition is a condensation of the anisotropic fluid, with droplets extending into contiguous channels.

On the other hand, recent experiments of 4He adsorbed on bundles of singlewalled carbon nanotubes [40] shown the existence of different adsorption regimes. At low coverages, single and three 1D chains are formed along the grooves on the bundle surfaces. As the coverage is increased, the admolecules form a two-dimensional (2D) monolayer over the surface of the nanotube bundle thus exhibiting 1D to 2D crossover. Similar behavior has been observed in other systems where the adsorption occurs on the external surface of the nanotube bundle [42]. The existence of close parallel 1D lines of adsorbed atoms suggests the possibility of transverse interactions between neighbor lines.

As discussed in the previous paragraphs, regardless the adsorption-taking place in the interior of a nanotube, in interstitial channels or in the groove sites, the interaction between molecules in adjacent chains is essential to the formation of ordered phases at low temperatures. Then, it is of interest and of value to inquire how the transverse interaction between 1D chains influences the phase behavior of the adlayer. It is clear that a complete analysis of this field is a quite difficult subject. For this reason, the understanding of simple models with increasing complexity might be a help and a guide to establish a general framework for the study of this kind of systems. The present work represents an effort in that direction.

Here, we study a simplified lattice-gas model, which mimics a nanoporous environment. In this model, 1D chains of atoms were arranged in a triangular structure. We included longitudinal interactions between nearest-neighbor particles adsorbed along a single channel, w_L, and transverse energy between particles adsorbed across nearest-neighbor channels, w_T. The phase behavior depends on the values of these various energies. In fact, for $w_T = 0$ and $w_L \neq 0$, the adlayer behaves as a one-dimensional fluid, the model is exactly soluble, and no phase transition develops when short-ranged coupling between neighboring particles exists [1,7,47]. For $w_T \neq 0$ and $w_L = 0$, successive transverse planes are uncorrelated and the system is equivalent to the well-known two-dimensional triangular lattice. In this case, the phase diagram has been widely studied for both attractive [48,49] and repulsive nearest-neighbor interactions [48-51]. In the more general case ($w_T \neq 0$ and $w_L \neq 0$), a competition between interactions along a single channel (w_L) and a transverse coupling between sites in neighboring channels (w_T) allows to evolve to a three-dimensional adsorbed layer. Although most of the works on the three-dimensional lattice gas have been devoted to attractive lateral interactions (see, for instance, Refs. [52-55]), there have been a few studies related to repulsive couplings between adatoms. In this context, the present paper is concerned with accurate low-temperature calculations of adsorption properties [56,57] and critical behavior [58] in systems with predominantly repulsive interactions.

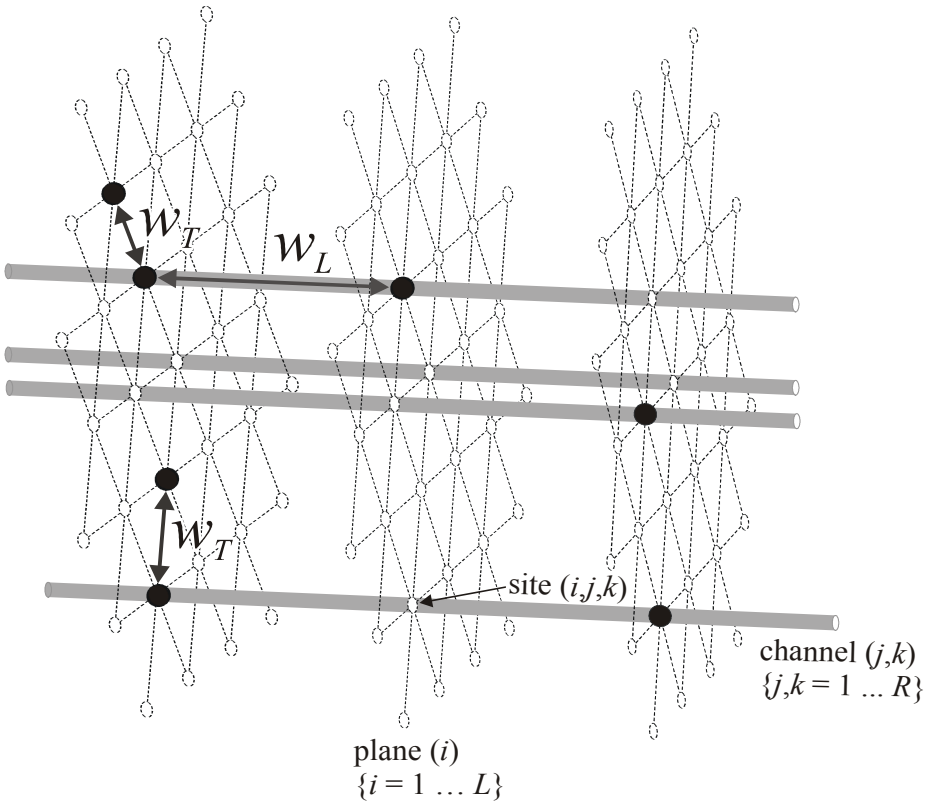

Fig. 1 Schematic representation of the studied system. Black and white circles correspond to occupied and empty sites, respectively.

Lattice-Gas Model and Monte Carlo Simulation Scheme

The Model. As it was discussed in the previous section, numerous experimental and theoretical studies of gas adsorption on carbon nanotube bundles predict the existence of close parallel channels of adatoms when the adsorption takes place (1) in the interior of a nanotube, (2) in interstitial channels, or (3) in the grooves site on bundle surfaces. In this context, we present a simplified lattice-gas model, where each channel or unit cell has been represented by a one-dimensional line of L adsorptive sites, with periodical boundary conditions. In order to include transverse interactions between parallel neighbor lines, these chains were arranged in a triangular

structure of size RxR and periodical boundary conditions. Under these conditions all lattice sites are equivalent hence border effects will not enter our derivation. The energies involved in the adsorption process are three:

(1) ε_o, interaction energy between a particle and a lattice site;
(2) w_L, interaction energy between adjacent occupied axial sites; and
(3) w_T, interaction energy between particles adsorbed on nearest-neighbor transverse sites.

Thus, the resulting substrate was an anisotropic three-dimensional array of M=LxRxR adsorption sites, where each site was surrounded by two "axial" sites along the chain's axis and six "transverse" sites belonging to nearest-neighbor unit cells (see Fig. 1).

In order to describe the system of N molecules adsorbed on M sites at a given temperature T, let us introduce the occupation variable $c_{i,j,k}$ which can take the following values: $c_{i,j,k}$ = 0 if the corresponding site (i,j,k) is empty and $c_{i,j,k}$ = 1 if the site is occupied by an adatom. Then, the Hamiltonian of the system is given by

$$H = w_L \sum_{\langle i,j,k;i',j',k'\rangle_L} c_{i,j,k}c_{i',j',k'} + w_T \sum_{\langle i,j,k;i',j',k'\rangle_T} c_{i,j,k}c_{i',j',k'} + (\varepsilon_o - \mu)\sum_{(i,j,k)}^{M} c_{i,j,k}\ , \qquad (1)$$

where $\langle i,j,k;\ i',j',k'\rangle_L$ ($\langle i,j,k;\ i',j',k'\rangle_T$) represents pairs of NN axial (transverse) sites and μ is the chemical potential.

Monte Carlo Simulation in the Grand Canonical Ensemble. The adsorption process is simulated through a grand canonical ensemble MC method (GCEMC) [59]. For a given value of the temperature T and chemical potential μ, an initial configuration with $N = M / 2$ particles adsorbed at random positions is generated. Then an adsorption–desorption process is started, where a site is chosen at random and an attempt is made to change its occupancy state with probability given by the Metropolis rule [60]:

$$W = \min\left[1, \exp\left(-\frac{\Delta H}{k_B T}\right)\right], \qquad (2)$$

where $\Delta H = H_f - H_i$ is the difference between the Hamiltonians of the final and initial states and k_B is the Boltzmann constant. A MC step (MCS) is achieved when M sites have been tested to change its occupancy state.

The approximation to thermodynamical equilibrium is monitored through the fluctuations in the number N of adsorbed particles; this is usually reached after discarding n_0 = 3x10^5 MCS, and the averages were taken over the next n = 3x10^5 MCS. At low temperatures, up to 10^6 MCS had to be used in order to let the system relax from metastable states.

Thermodynamic quantities, such as mean coverage θ and mean energy of the system U are obtained as simple averages:

$$\theta = \frac{1}{M}\sum_{i,j,k}\langle c_{i,j,k}\rangle \quad \text{and} \quad U = \langle H\rangle, \qquad (3)$$

where $\langle\cdots\rangle$ denotes the time average over n Monte Carlo simulation runs.

The differential heat of adsorption q_d can be obtained as follows. From the grand partition function $\Xi(\mu,T,M)$, a well-known relationship from the thermodynamics of adsorption can be derived [61]: $(\partial \ln z/\partial\beta)_{\langle N\rangle} = \partial\langle U\rangle/\partial\langle N\rangle$ where $\beta = 1/k_B T$ and $z = \exp(\mu/k_B T)/h^3(2\pi m k_B T)^{3/2}$. For an ideal gas, $z \to k_B TP$, P being the pressure. Finally [59,62,63],

$$q_d = RT^2\left(\frac{\partial \ln P}{\partial T}\right)_{\langle N\rangle} - RT = -\frac{\partial\langle U\rangle}{\partial\langle N\rangle} = -\frac{\langle UN\rangle - \langle U\rangle\langle N\rangle}{\langle N^2\rangle - \langle U\rangle^2}, \quad (4)$$

where R is the gas constant (R/k_B = Avogadro's number); $\langle UN\rangle, \langle U\rangle, \langle N\rangle$ and $\langle N^2\rangle$ can be evaluated via GCEMC.

Monte Carlo Simulation in the Canonical Ensemble: Simulated Tempering Method. In order to study the critical behavior of the system, we have used an exchange MC method [64,65]. As in Ref. [64], we build a compound system that consists of m noninteracting replicas of the system concerned. The ith replica is associated with a heat bath at temperature T_i (or $\beta_i = 1/k_B T_i$). To determine the set of temperatures T_i, we set the highest temperature T_1 in the high-temperature phase where relaxation (correlation) time is expected to be very short and there exists only one minimum in the free energy space. On the other hand, the lowest temperature T_m is set in the low-temperature phase whose properties we are interested in. Finally, the difference between two consecutive temperatures, T_i and T_{i+1} with $T_i > T_{i+1}$, is set as $\Delta T = (T_1 - T_m)/(m-1)$ (equally spaced temperatures).

Under these conditions, the algorithm to carry out the simulation process is built on the basis of two major subroutines:

(i) *Replica update*. Interchange vacancy particle. The procedure is as follows. (a) One out of the m replicas is randomly selected (for example, the ith replica). (b) A monomer and an empty site, both belonging to the replica chosen in (a), are randomly selected and their coordinates are established. Then, an attempt is made to interchange its occupancy state with probability given by the Metropolis rule [60], $W = \min[1, \exp(-\Delta H/k_B T)]$.

(ii) *Exchange*. Exchange of the two configurations X_i and X_j, corresponding to the ith and i'th replicas, respectively, is tried and accepted with probability $W(X_i, \beta_i \mid X_{i'}, \beta_{i'})$. In general, the probability of exchanging configurations of the ith and i'th replicas is given by [64]

$$W(X_i, \beta_i \mid X_{i'}, \beta_{i'}) = \begin{cases} 1 & \text{for } \Delta \le 0 \\ \exp(-\Delta) & \text{for } \Delta > 0 \end{cases}, \quad (5)$$

where $\Delta = (\beta_i - \beta_{i'})[H(X_{i'}) - H(X_i)]$. As in Ref. [64], we restrict the replica exchange to the case $i = i+1$.

The complete simulation procedure is the following: (1) initialization, (2) replica update, (3) exchange, and (4) repeat from step (2), $m \times M$ times. This is the elementary step in the simulation process or Monte Carlo step (MCS). The initialization of the compound system of m replicas, step (1), is as follows. By starting with a random initial condition, the configuration of replica 1 is obtained after n_1 MCS' at T_1 (MCS' consists of M realizations of the replica update subroutine). Second, for $i = \{2, \ldots, m\}$, the configuration of the ith replica is obtained after n_1 MCS' at T_i, taking as initial condition the configuration of the replica to T_{i-1}. This method results more efficient than a random initialization of each replica.

Procedures (1)–(4) are repeated for all lattice sizes. For each lattice, the equilibrium state can be well reproduced after discarding the first n_2 MCS. Then, averages are taken over n_{MCS} successive MCS. As was mentioned above, a set of equally spaced temperatures is chosen in order to accurately calculate the physical observables in the close vicinity of T_c.

The thermal average $\langle \cdots \rangle$ of a physical quantity A is obtained through simple averages,

$$\langle A\rangle = \frac{1}{n_{MCS}} \sum_{t=1}^{n_{MCS}} A[X_i(t)]. \quad (6)$$

In the last equation, X_i stands for the state of the ith replica (at temperature T_i).

All calculations were carried out using the BACO parallel cluster (composed by 60 PCs each with a 3.0 GHz Pentium-4 processor) located at Laboratorio de Ciencias de Superficies y Medios Porosos, Universidad Nacional de San Luis, San Luis, Argentina.

As it is standard for order-disorder phase transitions, a related order parameter was defined. In particular, at $\theta = 1/3$ [$2/3$], a $(\sqrt{3}\times\sqrt{3})$ [$(\sqrt{3}\times\sqrt{3})$*] ordered structure is formed in the planes below the critical temperature. Depending on the sign of the longitudinal interactions, the order is propagated to all planes. For repulsive w_L, adatoms avoiding configurations with nearest-neighbor interactions order along the channels in a structure of alternating particles separated by empty sites. On the other hand, attractive monomer-monomer longitudinal interactions favor the formation of pairs of nearest-neighbor adsorbed particles along the lines.

For the case of repulsive longitudinal interactions, Fig. 2a shows two successive planes, k and $k+1$, for one possible configuration of the phase appearing at critical regime and $\theta = 1/3$. Due to the periodic boundary conditions the degeneracy of this "local phase" is equal to 6. These configurations allow us to decompose the "local lattice" into six different sublattices (see Figs. 2b and 2c)*. The coverage on each sublattice is denoted as $\theta_s (s = 1,....,6)$. In this way, a "local order parameter", φ_k, can be defined as

$$\varphi_k = \sum_{s,t;\, s\neq t} |\theta_s - \theta_t|, \tag{7}$$

where we sum the differences (absolute value) between the coverage corresponding to two sublattices.

When the system is disordered ($T > T_c$), all sublattices are equivalents and the order parameter is minimum. However, when a configuration of the local phase appears at $T < T_c$, this is allocated on a sublattice. Let us suppose that this configuration lies on the sublattice s. Then, the coverage θ_s is maximum (θ_s =1) and the coverage of the rest of the sublattices is minimum. Consequently, φ_k is also maximum. On the basis of φ_k, the generalized order parameter, φ, can be written as

$$\varphi = A\sum_{k=0}^{L} \varphi_k, \tag{8}$$

where A is a normalization factor. The definition in Eq. 8 is computationally convenient and φ appears as a good order parameter evidencing the order-disorder phase transition.

In a similar way, it is possible to define the order parameter corresponding to θ = 2/3 and repulsive longitudinal interactions.

For attractive longitudinal interactions, it is not appropriate to define local sublattices. In this case, each sublattice s $(s = 1,....,3)$ lies on the total lattice (see Fig. 3) and φ can be easily defined as $\varphi = |\theta_1 - \theta_2| + |\theta_1 - \theta_3| + |\theta_2 - \theta_3|$.

Now, the reduced fourth-order cumulant, $U_{R[L]}$, introduced by Binder [66] and related to the order parameter, can be calculated as

* By inspecting Fig. 2, it is possible to note that the configuration presented in Fig. 2a was formed on the sublattice 1.

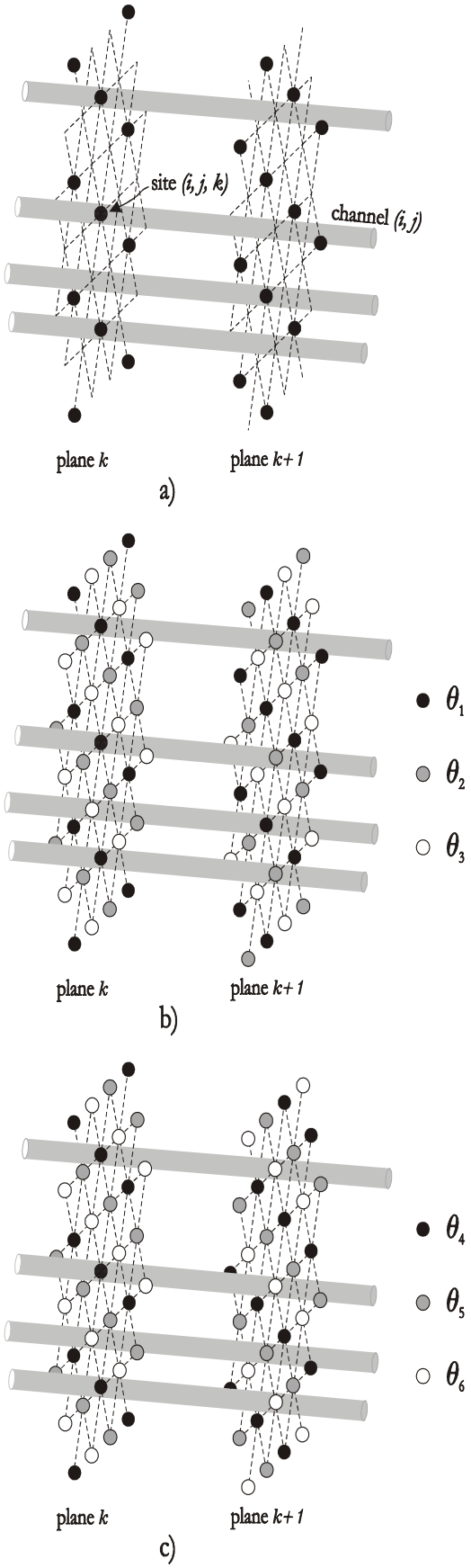

Fig. 2 (a) Snapshot of two successive planes, k and k+1, for a possible configuration of the ordered phase appearing at θ=1/3 and repulsive longitudinal interactions. The solid circles represent occupied sites. The different sublattices used in order to define a local order parameter characterizing this low temperature structure are shown in parts (b) and (c).

$$U_{R[L]}(T) = 1 - \frac{\langle \varphi^4 \rangle_T}{3\langle \varphi^2 \rangle_T^2}, \tag{9}$$

where U_R *[*U_L*]* represents the cumulant obtained by variable R *[*L*]* and fixed L *[*R*]*. The thermal average $\langle \cdots \rangle_T$, in all the quantities, means the time average throughout the MC simulation.

The standard theory of finite-size scaling [66-68] allows for various efficient routes to estimate T_c from MC data. One of these methods, which will be used here, is from the temperature dependence of $U_{R[L]}(T)$, which is independent of the system size for $T = T_c$. In other words, T_c is found from the intersection of the curve $U_{R[L]}(T)$ for different values of R [L], since $U_{R[L]}(T_c)$ = const.

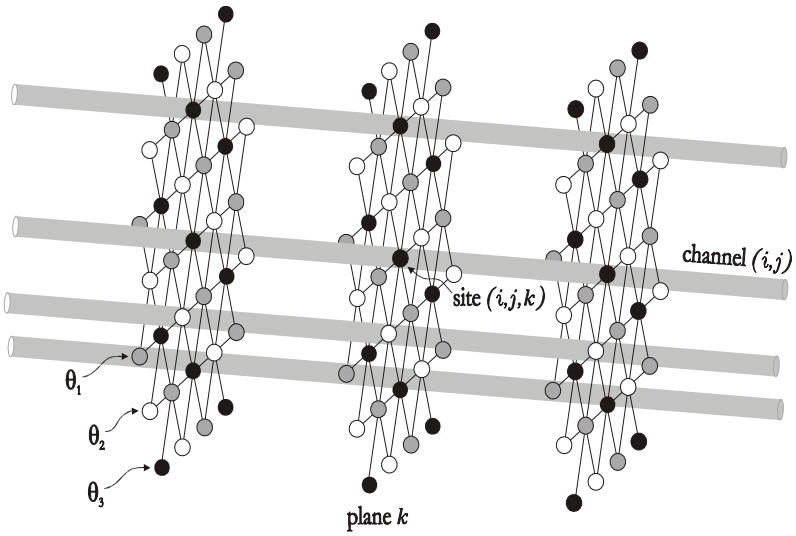

Fig. 3 Different sublattices defined for attractive longitudinal interactions and θ=1/3.

Thermodynamic Integration Method in the Canonical Ensemble. Let us suppose a lattice-gas of N interacting particles, each of which occupies one site on a regular lattice with M sites at temperature T. Then, it is possible to write

$$\left(\frac{\partial S}{\partial T}\right)_{N,M} = \frac{1}{T}\left(\frac{\partial U}{\partial T}\right)_{N,M}, \tag{10}$$

where S and U represent the configurational entropy and the internal energy, respectively. From Eq. 10,

$$S(N,M,T) = S(N,M,T_0) + \int_{T_0}^{T} \frac{dU}{T}. \tag{11}$$

Eq. 11 allows to calculate the entropy in different equilibrium states if $S(N,M,T_0)$ (reference state) and the integral in the second term are known. This procedure is called thermodynamic integration.

In our case, the determination of the entropy in the reference state is trivial. In fact, for a monoatomic lattice gas,

$$\lim_{T_0 \to \infty} S(N,M,T_0) = k_B \ln \binom{M}{N} = k_B \ln \left[\frac{M!}{N!(M-N)!}\right], \tag{12}$$

By using the Stirling's approximation $(\ln x! \approx x \ln x - x)$, Eq. 12 can be written as $s(\theta, T_0 \to \infty)/k_B = -\theta \ln \theta - (1-\theta)\ln(1-\theta)$, where $s \equiv S/M$ denotes the entropy per site.

On the other hand, the integral in the second term of Eq. 11 can be accurately obtained by evaluating U, at constant coverage, as a function of T. In order to get U, the procedure of MC simulation described in the previous section is performed. Then, $U(T)$ is spline fitted and numerically integrated [20].

In the next section, we will analyze the application of this methodology for calculating the entropy of interacting particles adsorbed on one-dimensional channels arranged in a triangular structure.

Results

Adsorption. In MC simulations, the system is represented by a unit cell of sites that is repeated periodically. As it was demonstrated by different authors studying adsorption in a porous medium [37,38,46,69,70], a small cell size is enough to simulate the one-dimensional channels. Then, we choose L = 96 in the direction along the axis of the nanotubes. On the other hand, the choice of appropriate sizes in the transversal direction has to be done in such a way that the ordered structures developing at criticality are not disturbed. In our case, lattices with R = 60 sites were used. With this lattice size we verified that finite-size effects, which affect the thermodynamical properties in the case of repulsive interactions at much smaller sizes, are negligible.

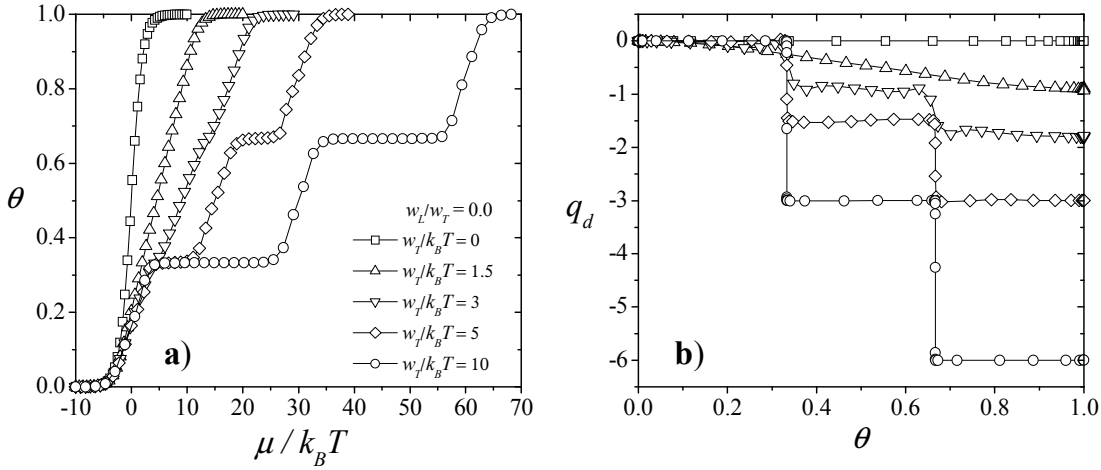

Fig. 4 Adsorption isotherm a), and differential heat of adsorption b), for $w_L/w_T = 0$ and different values of $w_T / k_B T$ as indicated.

We focus on the case of repulsive transversal interaction energy among the adsorbed particles $(w_T > 0)$. This is far more interesting since, as we shall see, a rich variety of ordered phases are observed in the transversal planes. In addition, repulsive and attractive axial lateral interactions were considered. As it can be easily demonstrated, the behavior of the system is completely determined by two parameters: w_L / w_T and $w_T / k_B T$. In our calculations, we can consider $w_T = 1$, in such a way that the system is characterized by two nondimensional parameters w_L and $k_B T$.

As indicated above, the adsorption process is simulated through a GCEMC method. In order to understand the basic phenomenology, in Fig. 4a we consider adsorption isotherms and in Fig. 4b differential heat of adsorption for null longitudinal interactions $(w_L / w_T = 0)$ and different values of $w_T / k_B T$ (= 0; 1.5; 3; 5 and 10). In this case, successive planes are uncorrelated and the system is equivalent to the well-known triangular lattice in two dimensions.

In the limit $w_T / k_B T \to 0$, the coverage grows monotonically with chemical potential and the corresponding isotherm is Langmuir type. For higher values of $w_T / k_B T$ (see for example $w_T / k_B T = 10$), three regimes appear in the isotherms. This behavior can be interpreted as follows: (i) for $0 < \theta < \frac{1}{3}$, the adatoms do not interact with each other and the adsorption sites are filled until the $(\sqrt{3} \times \sqrt{3})$ ordered phase is formed on them; (ii) for $\frac{1}{3} < \theta < \frac{2}{3}$, the filling continues up to the $(\sqrt{3} \times \sqrt{3})^*$ structure appearing on the lattice; and (iii) for $\frac{2}{3} < \theta < 1$, the surface is totally covered.

The plateaus in the adsorption isotherms, which are clearly associated to different structural rearrangements of the adsorbate molecules, are accompanied by characteristic signals in the differential heat of adsorption. In fact, a plateau in the isotherm appears as a step in the differential heat of adsorption. This behavior is shown in part b), confirming the discussion of part a). An example follows in order to make this point clear. The regimes described above for the adsorption isotherm with $w_T / k_B T = 10$ ($w_T = 1$ and $k_B T = 0.1$) can be reinterpreted by analyzing the differential heat of adsorption: from $\theta = 0$ to $\theta = \frac{1}{3}$, the particles are adsorbed avoiding nearest-neighbor interactions, which gives $q_d = 0$; from $\theta = \frac{1}{3}$ to $\theta = \frac{2}{3}$, each incoming particle is allocated on the lattice with three occupied nearest-neighbor sites in the plane and $q_d = 3w_T$. Finally, from $\theta = \frac{2}{3}$ to $\theta = 1$, to adsorb a new monomer it is necessary to occupy an empty site on the $(\sqrt{3} \times \sqrt{3})^*$ structure, this process involves an energy variation of $q_d = 6w_T$.

In Figs. 5 and 6, we set $w_T = k_B T = 10$ and vary the longitudinal interactions w_L/w_T (= -1.00;-0.75; -0.50; -0.25; 0; 0.25; 0.50; 0.75 and 1.00). For repulsive interactions (Fig. 5), a new plateau (step) appears in the adsorption isotherm (differential heat of adsorption) at $\theta = 0.5$ as w_L/w_T is increased. This behavior indicates the presence of an ordered structure at half coverage. In fact, planes are filled up to $\theta = 0.5$ with mean energy per site equal to $w_T/2$ (each adsorbed particle is surrounded by two occupied nearest-neighbors in the plane). Then, successive planes are occupied avoiding the formation of monomer-monomer pairs along the nanotubes. In this way, each plane is surrounded by two complementary planes [a complementary plane is obtained under the simultaneous inversion of all occupation variables ($c_{i,j,k} = 0 \to c_{i,j,k} = 1$ and $c_{i,j,k} = 1 \to c_{i,j,k} = 0$)] and the occupation of the channels consists of alternating particles separated by empty sites.

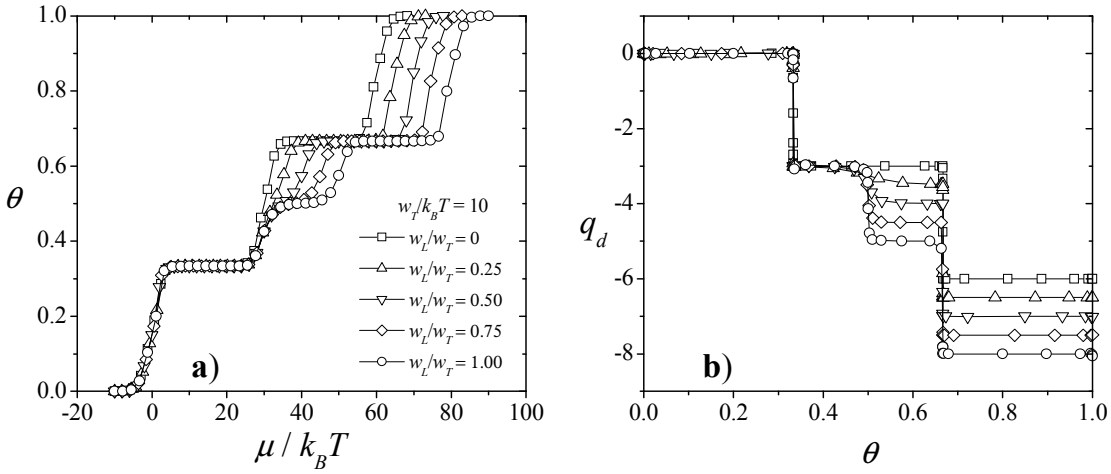

Fig. 5 Adsorption isotherm a), and differential heat of adsorption b), for $w_T/k_B T = 10$ ($w_T = 1$ and $k_B T = 0.1$) and different values of $w_L/w_T > 0$ as indicated.

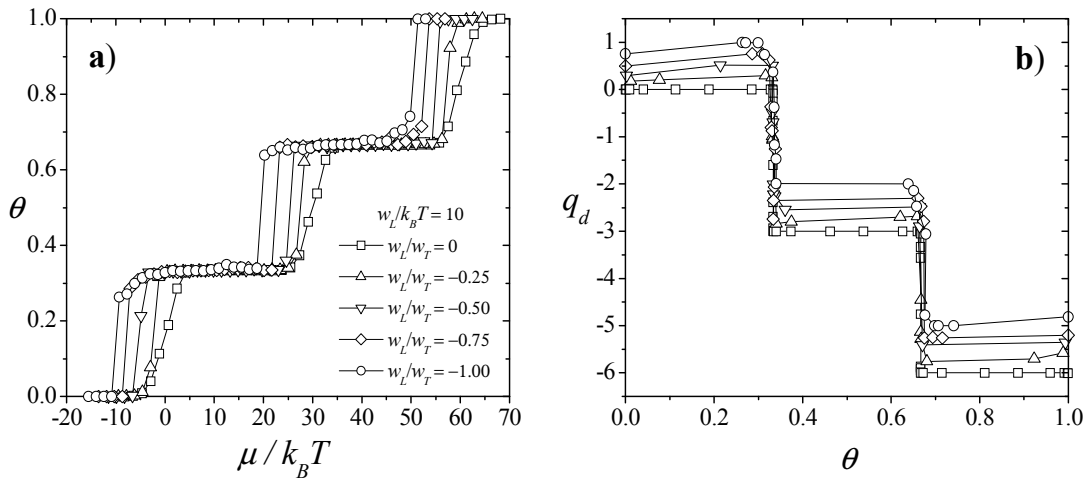

Fig. 6 Adsorption isotherm a), and differential heat of adsorption b), for $w_T/k_BT = 10$ ($w_T = 1$ and $k_BT = 0.1$) and different values of $w_L/w_T < 0$ as indicated.

At $\theta = \frac{1}{3}$, a $(\sqrt{3}\times\sqrt{3})$ ordered structure is formed in the planes for all values of w_L/w_T with mean energy per site equal to 0. Then, adatoms avoiding configurations with nearest-neighbor interactions order along the channels in a structure of alternating particles. The behavior of the system at $\theta = \frac{2}{3}$ can be understood from the equivalence vacancy particle.

On the other hand, as is shown in Fig. 6, attractive monomer-monomer longitudinal interactions favor the formation of pairs of nearest-neighbor adsorbed particles along the nanotubes. Consequently, the $(\sqrt{3}\times\sqrt{3})$ and $(\sqrt{3}\times\sqrt{3})^*$ ordered phases "propagate" along the channels and the plateaus (steps) in the adsorption isotherm (differential heat of adsorption) are reinforced. As it can be observed, the competition between repulsive transversal interactions and attractive longitudinal interactions yields an increase in the simulation error. Thus, the curves in Fig. 6 were obtained for $n_0 = n \approx 10^6$, with an effort of reaching almost the limits of our computational capabilities.

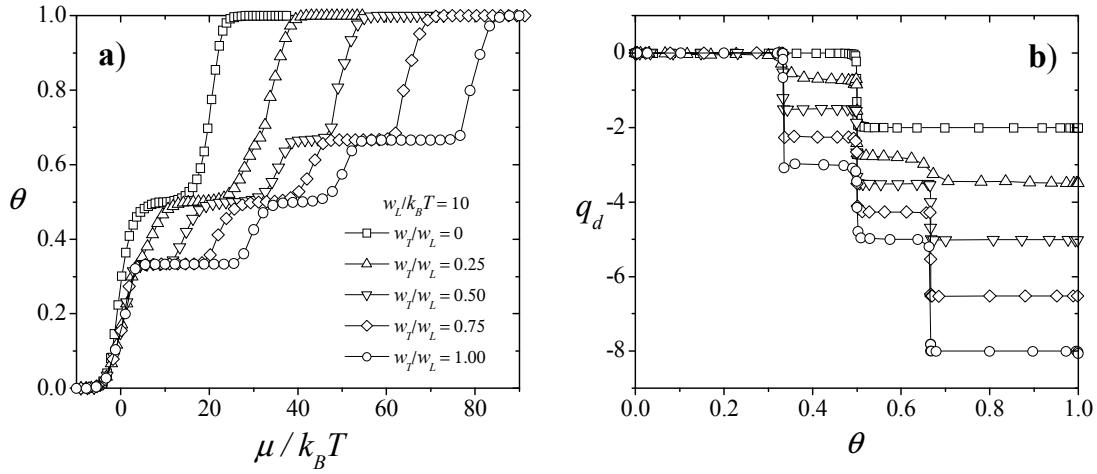

Fig. 7 Adsorption isotherm a), and differential heat of adsorption b), for $w_L/k_BT = 10$ ($w_L = 1$ and $k_BT = 0.1$) and different values of $w_T/w_L > 0$ as indicated.

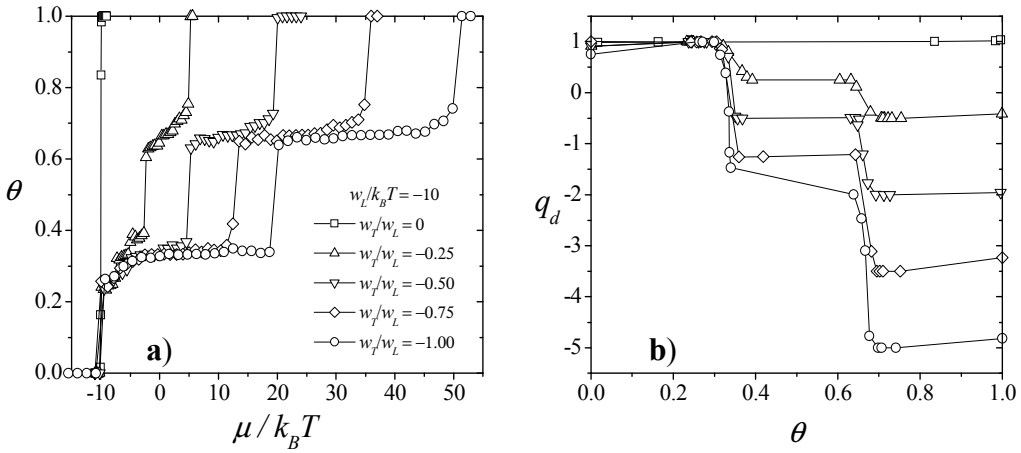

Fig. 8 Adsorption isotherm a), and differential heat of adsorption b), for $w_L/k_BT = 10$ ($w_L =$ 1 and $k_BT = 0.1$) and different values of $w_T/w_L < 0$ as indicated.

To complete our analysis, we study the effect of varying the transversal lateral interaction as the longitudinal interaction is fixed. For this purpose, the two limit cases in Figs. 5 and 6, the first $w_L / k_BT = 10$ and $w_T / w_L = 1$ (open down triangles) and the second $w_L / k_BT = -10$ and $w_T / w_L = -1$ (solid down triangles), are taken as starting point and, then, the transversal repulsive interaction is diminished while w_L / k_BT remains constant. Results for repulsive and attractive longitudinal interactions are shown in Figs. 7 and 8, respectively. In both cases, the adlayer changes from a three-dimensional fluid for $|w_T / w_L| > 0$ to a one-dimensional fluid for $w_T / w_L = 0$. For repulsive longitudinal energies and null transversal interactions, the isotherm develops a neat step at θ = 0.5. Adparticles avoiding configurations with nearest-neighbor repulsive heads order in the channels in a structure of alternating adatoms separated by an empty site. On the other hand, for attractive longitudinal energies and null transversal interactions, adsorption along the channels is favored and a typical stepped isotherm is obtained. In all cases, differential heat of adsorption follows the behavior of the isotherms. As it was discussed in Fig. 6, the mixing of repulsive and attractive interactions notably affects the accuracy of the simulations.

Configurational Entropy. Here, the computational simulations have been performed in the canonical ensemble. As in the previous section, we chose L = 96 in the direction along the axis of the nanotubes, R = 60 in the transverse direction and w_T=1.

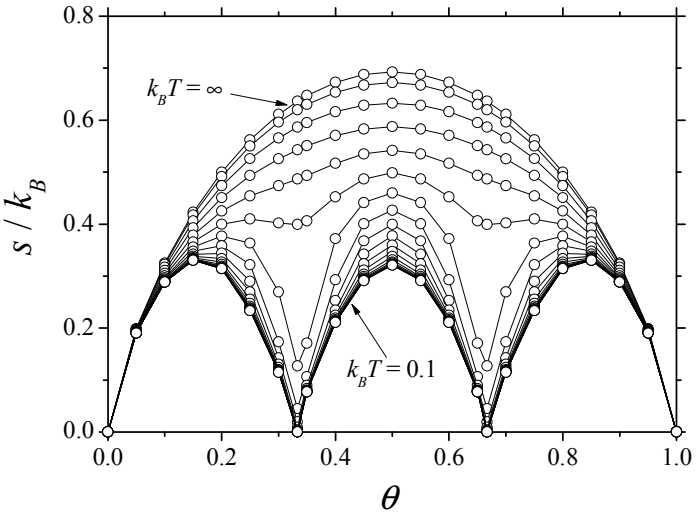

Fig. 9 Configurational entropy per site (in units of k_B) vs the surface coverage for interacting particles adsorbed in one-dimensional channels arranged in a triangular structure with w_T=1 and w_L=0. The curves from top to bottom correspond to the values of k_BT ranging from ∞ to 0.1.

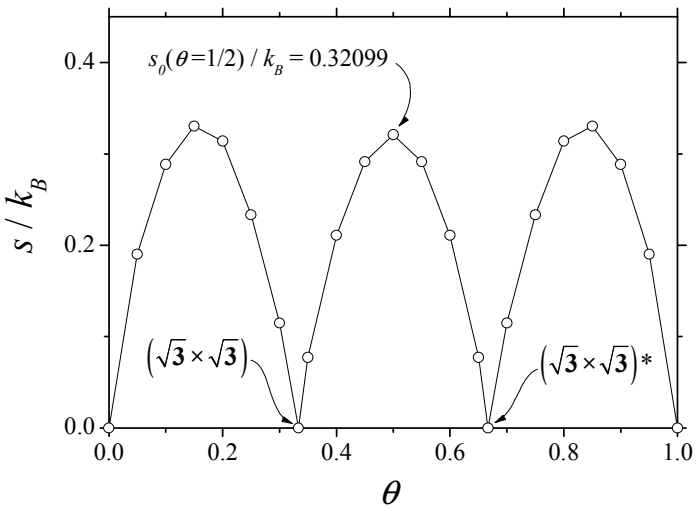

Fig. 10 Configurational entropy per site (in units of k_B) vs the surface coverage for repulsive interacting particles adsorbed in a triangular lattice in the ground state (w_T =1, w_L =0, and $k_BT\rightarrow 0$).

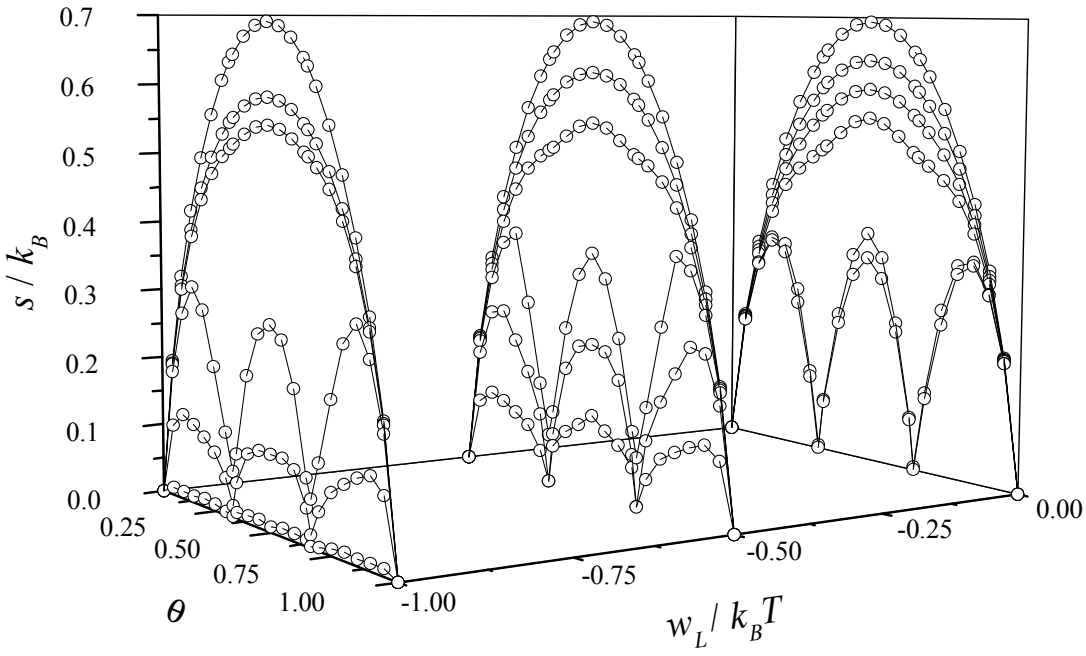

Fig. 11 Configurational entropy per site (in units of k_B) vs the surface coverage for w_T=1 and attractive values of w_L (= 0; −0.50; −1.00). For constant w_L, the curves from top to bottom correspond to the following: k_BT=∞, k_BT=0.95, k_BT=0.63, k_BT=0.47, k_BT=0.32, k_BT=0.19, and k_BT=0.1, respectively.

We firstly consider null axial interactions. Fig. 9 shows the canonical MC simulations of the configurational entropy per site s versus the surface coverage u for $w_L = 0$. As a consequence of the equivalence particle vacancy, the curves are symmetrical around $\theta = 0.5$. For high temperatures, the overall behavior can be summarized as follows: in the limits $\theta \rightarrow 0$ and $\theta \rightarrow 1$ the entropy tends to zero. For very low coverage $s(\theta)/k_B$ is an increasing function of θ, reaches a maximum at $\theta = 0.5$, then decreases monotonically to zero for $\theta > 0.5$.

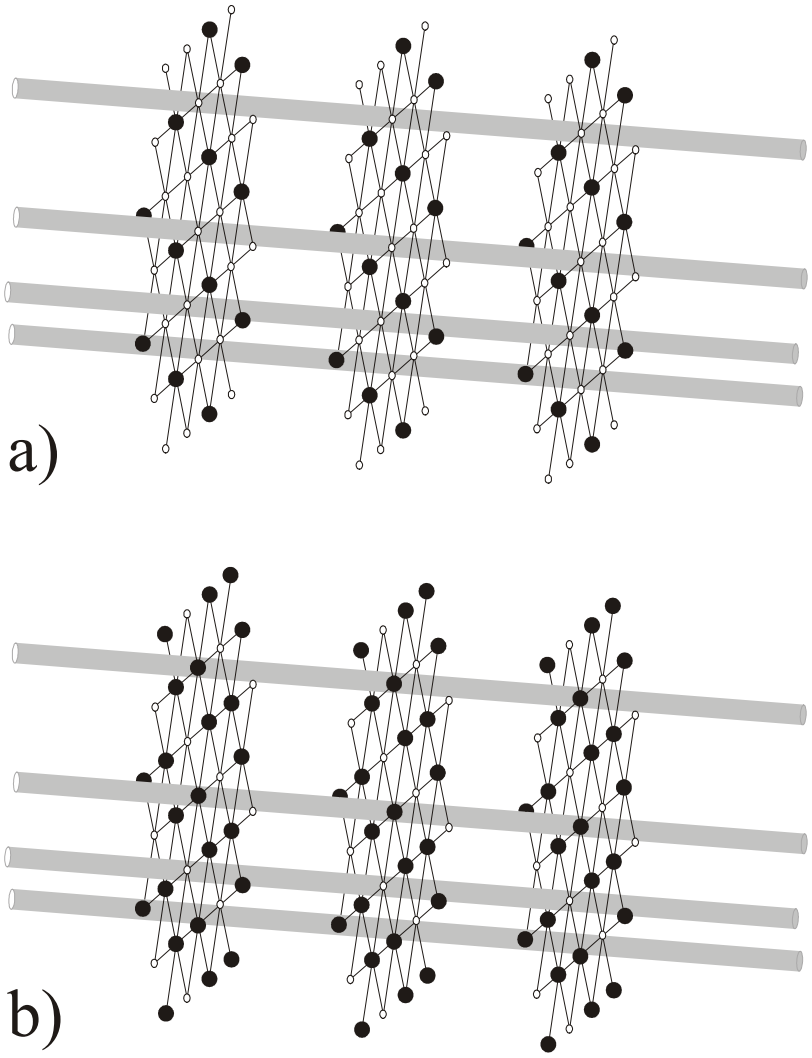

Fig. 12 Snapshots of the adsorbate at θ=1/3 (a) and θ=2/3 (b) for interacting particles adsorbed in one-dimensional channels arranged in a triangular structure with w_T=1, w_L < 0, and $k_BT \to 0$.

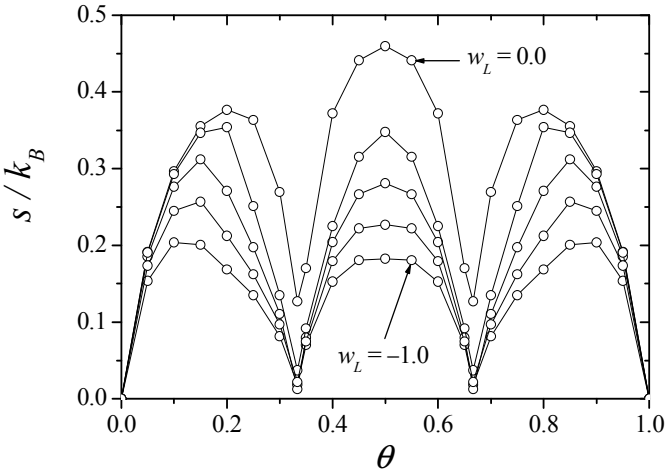

Fig. 13 Configurational entropy per site (in units of k_B) vs the surface coverage for w_T =1, k_BT=0.32, and attractive values of w_L (=0; −0.25; −0.50; −0.75; −1.00).

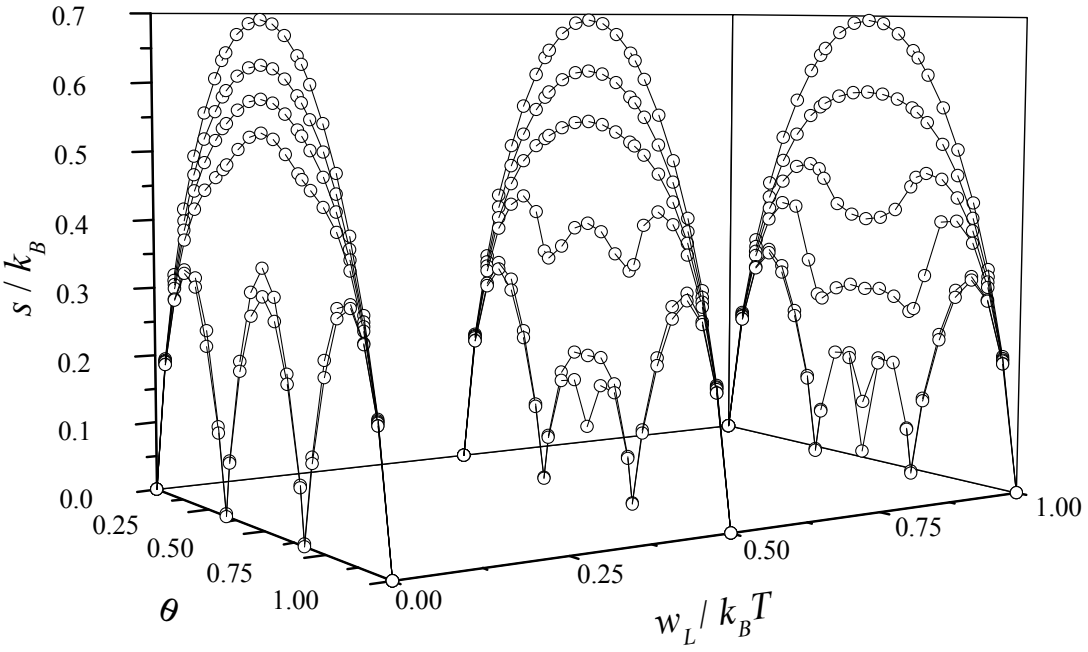

Fig. 14 Same as Fig. 11 for repulsive values of w_L (=0; 0.50; 1.00).

As the temperature is diminished, the entropy decreases for all coverage and develops two local minima at θ=1/3 and θ=2/3. In the ground state, $s(\theta = 1/3,\ T = 0)/k_B = s(\theta = 2/3,\ T = 0)/k_B = 0$ (see Fig. 10). These singularities provide valuable information about the phase behavior of the system. Precisely, they indicate the formation of ordered structures in the adlayer [$(\sqrt{3}\times\sqrt{3})$ structure at θ= 1/3 and $(\sqrt{3}\times\sqrt{3})^*$ structure at θ= 2/3). In addition, they are boundaries among three different adsorption regimes: (i) for $0 < \theta < \frac{1}{3}$, the lattice sites are filled until the $(\sqrt{3}\times\sqrt{3})$ ordered phase is formed on them; (ii) for $\frac{1}{3} < \theta < \frac{2}{3}$, this process continues up to the $(\sqrt{3}\times\sqrt{3})^*$ structure is completed; and (iii) for $\frac{2}{3} < \theta < 1$, the full coverage of the lattice is reached. The results in Figs. 9 and 10 match previous studies for triangular lattices (see for instance Refs. [71,72] and validate the MC scheme.

We now discuss the case corresponding to attractive axial interactions and different values of k_BT. For the sake of clarity, the analysis will be carried out in two parts. On the one hand, for constant w_L (= 0; −0.5; −1.00) and variable values of k_BT (= ∞ ; 0.95; 0.63; 0.47; 0.32; 0.19; 0.10), each set of curves presents two minima in the entropy as k_BT decreases (see Fig. 11). Same as in Fig. 9, the existence of these minima is associated to the formation of ordered structures in the adlayer. In this case, attractive axial interactions favor the formation of pairs of nearest-neighbor adsorbed particles along the nanotubes. Consequently, the $(\sqrt{3}\times\sqrt{3})$ and $(\sqrt{3}\times\sqrt{3})^*$ phases "propagate" along the channels and emerge the structures, as shown in Fig. 12.

On the other hand, for constant k_BT and variable values of w_L, the entropy diminishes over the whole range of converge as $|w_L|$ is increased. This situation can be clearly visualized in Fig. 13, where a typical case of constant k_BT (= 0.32) and variable w_L (= 0; −0.25; −0.5; −0.75; −1.00) is plotted. The position of the total maximum at θ= 0.5 is independent of w_L, while the position of the local maximum at low (high) coverage tends to θ= 0.2 (θ= 0.8) from the left (right) as w_L tends to −1.

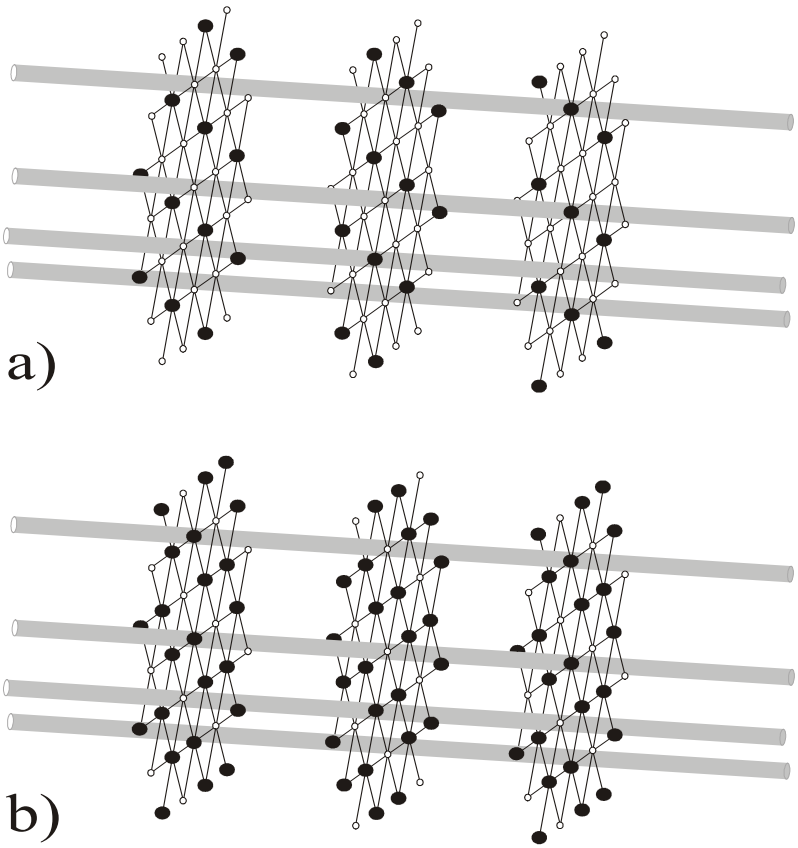

Fig. 15 Snapshots of the adsorbate at θ=1/3 (a) and θ=2/3 (b) for interacting particles adsorbed in one-dimensional channels arranged in a triangular structure with w_T=1, w_L>0, and $k_BT \to 0$.

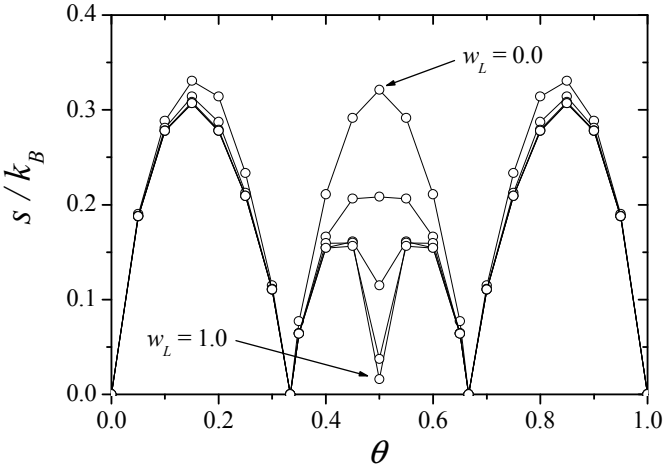

Fig. 16 Same as Fig. 13 for w_T=1, k_BT=0.1, and repulsive values of w_L (=0; 0.25; 0.50; 0.75; 1.00).

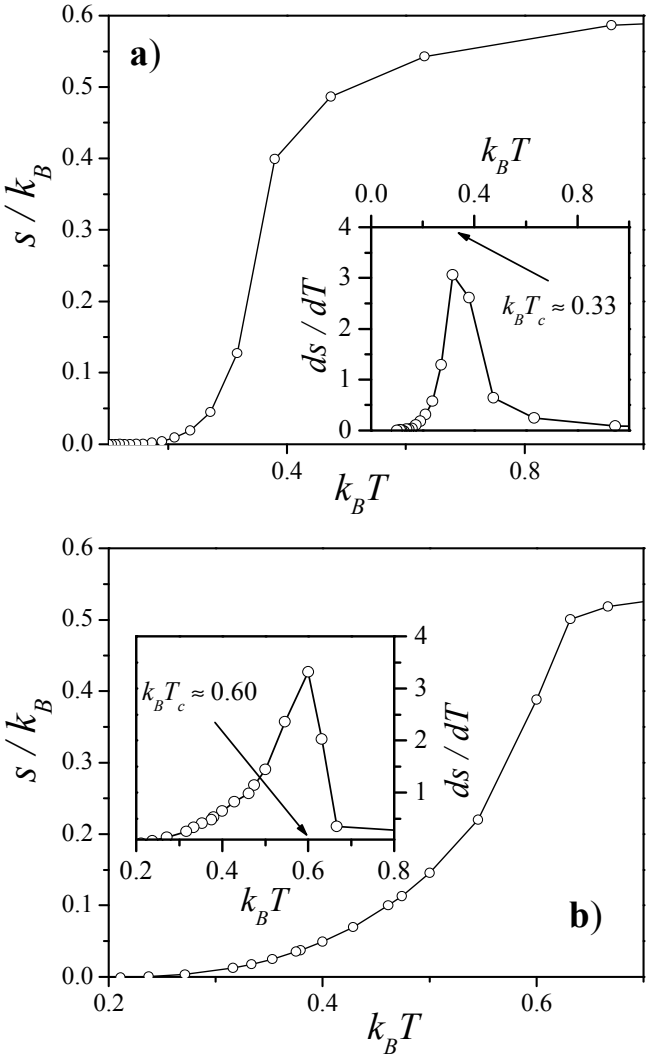

Fig. 17 Configurational entropy per site (in units of k_B) as a function of temperature at the critical coverage. In the inset we have plotted the corresponding derivative showing a peak in the critical temperatures. (a) w_T=1, w_L=0, and θ=1/3. (b) w_T=1, w_L=−0.5, and θ=1/3.

We now turn to repulsive axial interactions, which present an interesting behavior, as shown in Fig. 14. Thus, for constant w_L (= 0; 0.5; 1.00) and variable values of k_BT (= ∞; 0.95; 0.63; 0.47; 0.32; 0.19; 0.10), three minima appear in the entropy as T decreases. This can be rationalized as follows: at θ = 1/3 [2/3], a $(\sqrt{3}\times\sqrt{3})$ [$(\sqrt{3}\times\sqrt{3})$*] ordered structure is formed in the transversal planes below the critical temperature. In addition, given that $w_L > 0$, particles avoiding configurations with nearest-neighbor axial interactions develop a structure of alternating particles along the channels. Snapshots in Figs. 15 a) and 15 b) correspond to two possible configurations of the phase appearing at critical regime for θ = 1/3 and θ = 2/3, respectively. The degeneracy of such structures is $3\times 2^{(L-1)}$, and, consequently, $s(\theta = 1/3,\ T = 0)/k_B = s(\theta = 2/3,\ T = 0)/k_B = 0$.

As discussed in the previous section, at θ = 1/2 the situation is more complex. In this case, each transverse plane is surrounded by two complementary planes* and the occupation of the channels consists of alternating particles separated by empty sites. Then, the main contribution to the entropy per site comes from the number of different ways, Ω, to arrange the particles on the planes at half coverage with mean energy per site equal to w_T /2. This quantity can be obtained from calculations

* A complementary plane is obtained under the simultaneous inversion of all occupation variables ($c_{i,j,k}$=0 → $c_{i,j,k}$=1 and $c_{i,j,k}$=1 → $c_{i,j,k}$=0).

of entropy per site for triangular lattices at $\theta = 0.5$. In Fig. 10, we presented such calculations for a triangular lattice of side R. As it can be observed, $\ln \Omega = aR^2$, being a=0.32099. In addition, a factor of 2 must be added in order to include the effect of the complementarity along the channels. Then, in the thermodynamic limit $(L = R \to \infty)$, $s_0(1/2) \propto \text{const}\, R^2/(LR^2) = 0$.

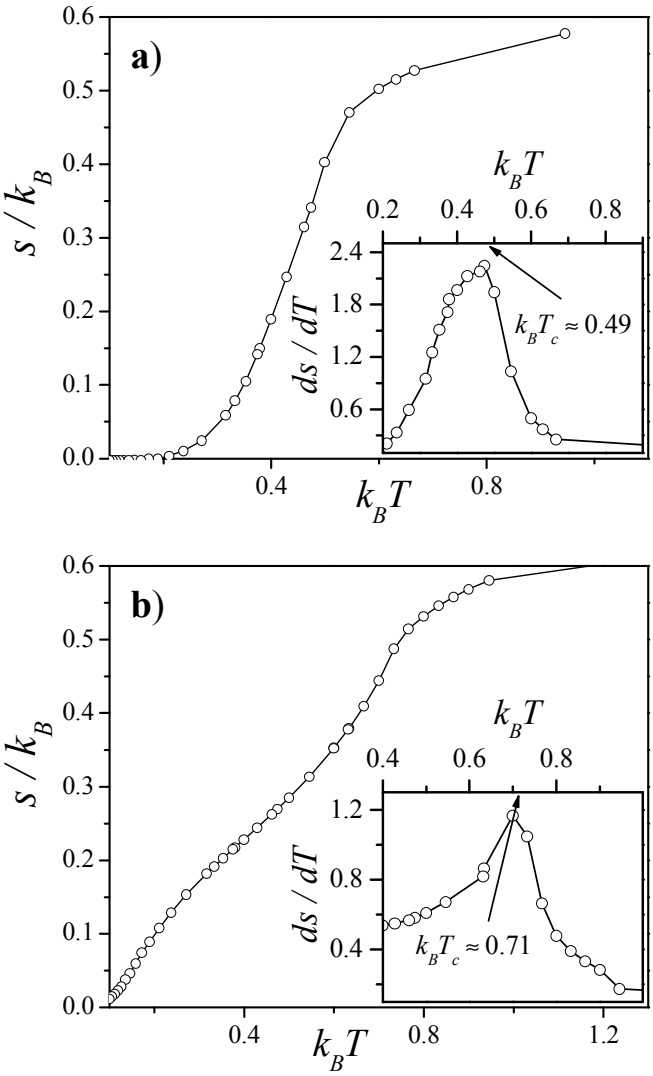

Fig. 18 Configurational entropy per site (in units of k_B) as a function of temperature at the critical coverage. In the inset we have plotted the corresponding derivative showing a peak in the critical temperatures. (a) w_T=1, w_L=0.5, and θ=1/3. (b) w_T=1, w_L=1, and θ=1/2.

On the other hand, Fig. 16 shows the behavior of the configurational entropy as a function of coverage for constant k_BT (= 0.1) and variable values of w_L (= 0; 0.25; 0.5; 0.75; 1.00). The entropy diminishes over the whole range of coverage as w_L is increased.

Finally, the configurational entropy can be used to estimate the critical temperatures corresponding to the critical concentrations θ = 1/3, 1/2, and 2/3. Consequently, the dependence of s/k_B (and its derivative) on temperature was plotted. Some typical cases are shown in Figs. 17 and 18. The inflection point of $s(T)/k_B$ (peak in its derivative) determines the critical temperature. In the studied cases, the calculated values are shown in Table 1. For w_L = 0, the critical temperature obtained comes very close to the expected value of k_BT_c/w_T = 0.3355 corresponding to the triangular lattice [73], which indicates the degree of accuracy of the procedure used here.

Table 1 Critical temperatures corresponding to the critical coverage $\theta = 1/3$ (2/3) and 1/2. In all cases $w_T = 1$.

	k_BT_c/w_T	
w_L/w_T	$\theta = 1/3$ (2/3)	$\theta = 1/2$
−1.00	0.76	-
−0.75	0.67	-
−0.50	0.60	-
−0.25	0.48	-
0.00	0.33	-
0.25	0.42	0.41
0.50	0.49	0.53
0.75	0.54	0.63
1.00	0.59	0.71

Critical Behavior. In this section, the critical behavior of the present model have been investigated by means of MC simulations and finite-size scaling techniques [66-68]. As a consequence of the equivalence particle vacancy, the critical behavior at $\theta = 2/3$ is as at $\theta = 1/3$. Then, we restrict our calculations to $\theta = 1/3$. In addition, we set $w_T = 1$ and vary w_L/w_T from −1 to 1 $(-1 \le w_L / w_T \le 1)$.

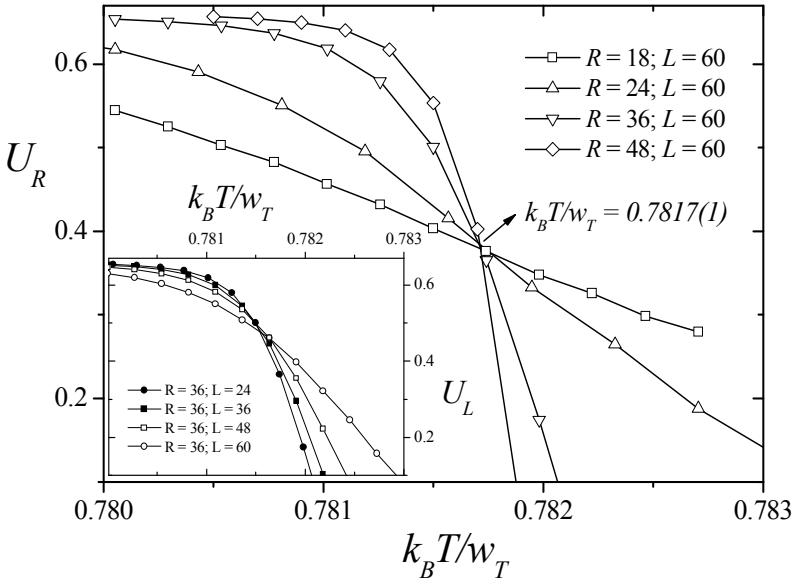

Fig. 19 $U_R(T)$ and $U_L(T)$ (inset) vs k_BT/w_T, for a typical case of $w_L < 0$: $\theta = 1/3$ and $w_L/w_T = -1$.

In the particular case of $w_L = 0$, successive planes are uncorrelated and the system is equivalent to the well-known triangular lattice. The value obtained of $k_BT_c/w_T = 0.3354(1)$ confirms this arguments and validates the MC scheme [73-76]. The data are not shown here for brevity.

Hereafter, we discuss the behavior of the critical temperature as a function of w_L/w_T. We start with the case of attractive longitudinal interactions. As an example, Fig. 19 illustrates the reduced four-order cumulants plotted versus k_BT/w_T for $w_L/w_T = -1$. From their intersections one gets the

estimation of the critical temperature. The lattice sizes used in the simulation* are compiled in Table 2 along with the values of the parameters in the simulated tempering runs. In the figure, the critical temperature is obtained from the curves of $U_R(T)$ (calculated for different values of R and fixed L). The resulting value, $k_BT_c/w_T = 0.7817(1)$, agrees very well with previous determinations obtained from the inflection on the function $s(T)$ (configurational entropy per site of the adlayer as a function of the temperature). Due to the finite-size scaling technique and the simulation procedure used in this case, the estimation of T_c in the present section is expected to be more accurate than that calculated in the previous section.

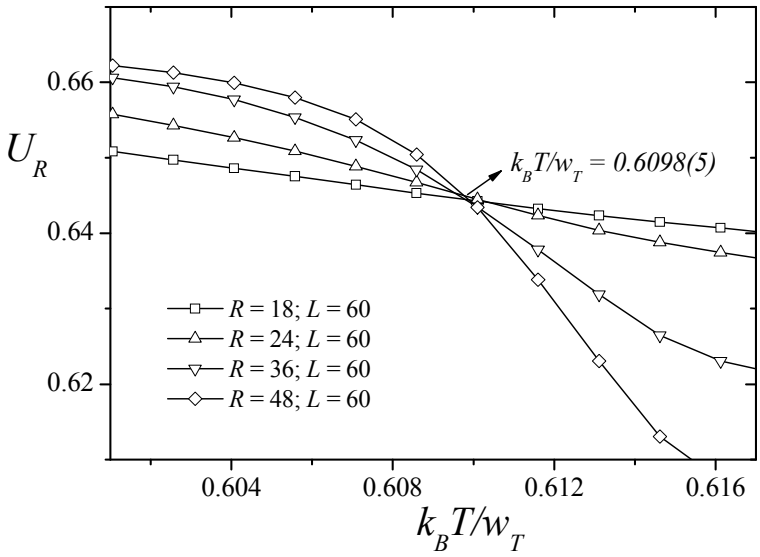

Fig. 20 $U_R(T)$ vs k_BT/w_T for θ=1/3 and w_L/w_T= 1.

Table 2 Parameters of the simulated tempering runs for two typical cases (w_L/w_T= −1, +1).

w_L/w_T	R	L	m	n_1	n_2	n_{MCS}	k_BT_{min}/w_T	k_BT_{max}/w_T
−1	18	60	12	10^3	10^5	10^5	0.780 053	0.782 705
	24	60	20	10^3	10^5	10^5	0.777 400	0.784 600
	36	60	12	10^3	10^5	10^5	0.780 053	0.782 705
	48	60	11	10^3	10^5	10^5	0.780 500	0.782 500
1	18	60	12	10^3	5×10^5	5×10^5	0.601 053	0.617 632
	24	60	12	10^3	5×10^5	5×10^5	0.601 053	0.617 632
	36	60	12	10^3	5×10^5	5×10^5	0.601 053	0.617 632
	48	60	12	10^3	5×10^5	5×10^5	0.601 053	0.617 632

The study was extended to repulsive longitudinal interactions. Fig. 20 shows the data for a typical case (w_L/w_T = 1), resulting k_BT_c/w_T= 0.6098(5), in well agreement with the value obtained in previous section ($k_BT_c/w_T \approx 0.59$). As indicated in Fig. 19, the parameters of the simulation are listed in Table II.

Due to the presence of anisotropy (the couplings are taken to be different in the different lattice directions), it is expected that the correlation functions in transverse and longitudinal directions may be governed by correlation lengths diverging with different critical exponents [77,78]. However, it is worth pointing out that we do not assume any particular value of the critical exponents for the

* As it is common in MC simulations, one represents the system with a unit cell of sites that is repeated periodically. Then, the choice of appropriate sizes in the transverse direction has to be done in such a way that the ordered structures are not disturbed.

transitions analyzed here in order to calculate their critical temperatures, since the analysis rely on order parameter cumulant's properties*. In addition, the procedure shown in Figs. 20 and 21 was repeated for the curves of $U_L(T)$, which were obtained for variable L and fixed R. As an example, Fig. 22 presents the results obtained for the case $w_L/w_T = -1$. As it is expected, identical results (within numerical errors) are obtained in both ways.

Finally, the calculations were carried out for $w_L/w_T = -0.75, -0.50, -0.25, 0.00, 0.25, 0.50$, and 0.75 and the results were collected in Table 3**. As it can be observed, the critical temperature presents a nontrivial behavior as a function of w_L/w_T. An understanding of the dependence of k_BT_c/w_T on w_L/w_T can be developed by following the subtle interdependence of energetic and entropic costs necessary to alter the ordered phase. This will be discussed in the next section.

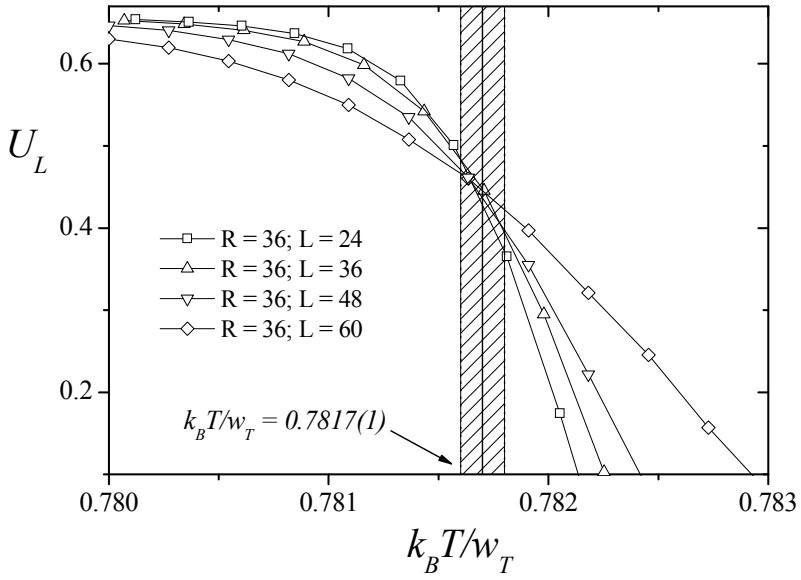

Fig. 21 $U_L(T)$ vs k_BT/w_T for θ=1/3 and $w_L/w_T = -1$.

Table 3 Critical temperatures corresponding to the critical coverage θ=1/3 (2/3). The data were obtained from the crossing of the cumulants.

w_L/w_T	k_BT_c/w_T θ=1/3 (2/3)
−1.00	0.7817(1)
−0.75	0.695(4)
−0.50	0.604(4)
−0.25	0.495(4)
0.00	0.3354(1)
0.25	0.436(1)
0.50	0.506(1)
0.75	0.562(1)
1.00	0.6098(5)

* A systematic analysis of critical exponents for each w_L/w_T was not carried out since this was out of the scope of the present work.

** The calculations for w_L/w_T=1.0 and w_L/w_T=−1.0 were carried out with an effort reaching almost the limits of our computational capabilities. In the case of intermediate values of w_L/w_T, the number of MCS was restricted in order to get results in a reasonably computational time. These conditions are reflected in the different values of the numerical errors reported in Table 3.

Theoretical Approach: Free Energy Minimization Criterion. Hereafter, we will use FEMCA [21] in order to discuss the dependence of k_BT_c/w_T vs w_L/w_T obtained from MC simulation.

In a closed system of adsorbed particles with repulsive interactions, the phase transition occurring in the adsorbate is a continuous (second-order) phase transition. In other words, the entropy, S, varies continuously from a completely ordered state (when $T \to 0$) to a disordered state (when $T \to \infty$). Around T_c, S changes abruptly (but continuously) [20]. Then, it is possible to analyze the phase transition taking into account the Helmholtz free energy, $F = U - TS$, in the two extreme states (maximum order and maximum disorder). Accordingly,

$$F_\infty = \lim_{T\to\infty} F \text{ and } F_0 = \lim_{T\to 0} F\,, \tag{13}$$

then

$$F_\infty << F_0 \Rightarrow T > T_c\,, \tag{14}$$

$$F_\infty >> F_0 \Rightarrow T < T_c\,, \tag{15}$$

$$F_\infty = F_0 \Rightarrow T \approx T_c\,. \tag{16}$$

The last equation allows to determine T_c. This calculation is not exact due to the system that does not pass from an extreme order to an extreme disorder. There exist intermediate states between the two extreme states. However, as we will show in the following analysis, Eq. 16 provides a very good approximation for T_c. Interested readers are referred to Ref. [21] for a more complete description of FEMCA.

In general, for a system of interacting particles at temperature T results

$$f_0 = u_0 - Ts_0 \text{ and } f_\infty = u_\infty - Ts_\infty\,, \tag{17}$$

where f, e and s represent the free energy per site, the mean energy per site and the entropy per site in the thermodynamical limit, respectively.

$$f = \lim_{M\to\infty}\frac{F}{M},\quad u = \lim_{M\to\infty}\frac{U}{M} \text{ and } s = \lim_{M\to\infty}\frac{S}{M}\,. \tag{18}$$

If $f_0 = f_\infty$, this is

$$u_0 - Ts_0 = u_\infty - Ts_\infty\,, \tag{19}$$

then $T \approx T_c$ and

$$T_c \approx \frac{\Delta u}{\Delta s} = \frac{u_\infty - u_0}{s_\infty - s_0}\,. \tag{20}$$

From Eq. 20, it is possible to calculate the critical temperature and to interpret the dependence of k_BT_c/w_T with w_L/w_T obtained from simulations. As in previous sections, we restrict the study to $\theta =$ 1/3 (2/3) and $-1 \le w_L/w_T \le 1$.

Case I: $\theta = 1/3$ and $w_L / w_T > 0$. In general, $u_\infty(\theta)$ can be calculated from mean-field approximation. Thus,

$$u_\infty(\theta) = \frac{1}{2M}(6N\theta w_T + 2N\theta w_L). \tag{21}$$

In this case $\theta = N/M = 1/3$, and

$$u_\infty(1/3) = \tfrac{1}{3} w_T + \tfrac{1}{9} w_L. \tag{22}$$

In order to calculate the entropy of the disordered state, the configurational factor of monomers Ω, is employed

$$\Omega = \frac{M!}{N!(M-N)!}. \tag{23}$$

Thus,

$$s_\infty = \lim_{M\to\infty} \frac{k_B \ln \Omega}{M}. \tag{24}$$

In the particular case of $\theta = 1/3$, the entropy per site of the disordered state results

$$s_\infty(1/3) = -k_B(\ln \tfrac{1}{3} + \tfrac{2}{3}\ln 2). \tag{25}$$

In addition, the mean energy per site and the entropy per site for the ordered state at $\theta = 1/3$ and $T = 0$ are $u_0(1/3) = s_0(1/3) = 0$. Then, the critical temperature depends on the mean energy and the entropy of the disordered state. From Eqns. 22, 25, and 20, we obtain $T_c(1/3)$:

$$T_c(1/3) \approx \frac{u_\infty(1/3)}{s_\infty(1/3)} \approx \frac{(1/3)w_T + (1/9)w_L}{-k_B[\ln(1/3) + (2/3)\ln 2]}. \tag{26}$$

Finally,

$$\frac{k_B T_c(1/3)}{w_T} \approx \frac{(1/3) - (1/9 w_L / w_T)}{-\ln(1/3) - (2/3)\ln 2} \quad (w_T > 0 \text{ and } w_L / w_T > 0). \tag{27}$$

Case II: $\theta = 1/3$ and $w_L / w_T < 0$. The mean energy and the entropy of the disordered system are as in Eqns. 21 and 24. On the other hand, for the ordered system, $s_0(1/3) = 0$ and $e_0(1/3) = w_L/3$. Then

$$\frac{k_B T_c(1/3)}{w_T} \approx \frac{(1/3) - (2/9 w_L / w_T)}{-\ln(1/3) - (2/3)\ln 2} \quad (w_T > 0 \text{ and } w_L / w_T < 0). \tag{28}$$

As it is expected, the calculations for $\theta = 2/3$ (do not shown here) provide identical results as cases I and II.

Fig. 22 shows the comparison between the simulated results previously presented in Table III and the theoretical predictions obtained from FEMCA for the critical temperature as a function of

w_L / w_T. The MC simulations reveal the main characteristics for the behavior of the critical temperature versus w_L / w_T: (i) the curve presents a minimum for $w_L / w_T = 0$, and (ii) for negative values of w_L / w_T, the critical temperatures are higher than the corresponding ones for positive w_L / w_T's. Both characteristics are very well reproduced by FEMCA.

The physical meaning of the main features of the critical temperature can be interpreted from the theoretical approach. In this framework, Eq. 20 shows that $k_B T_c / w_T$ depends on the mean energy and the entropy of the disordered state. The behavior of these quantities as a function of w_L / w_T allows to understand the arguments presented in the previous paragraph. Thus, the values of s_∞, s_0, and u_∞ are identical for repulsive and attractive longitudinal interactions. In addition, the magnitude of u_0 is constant ($u_0 = 0$) for $w_L > 0$ and increases with w_L ($u_0 = w_L/3$) for $w_L < 0$. Now we can interpret the difference between the two regimes in Fig. 22. From $-1 \le w_L / w_T \le 1$, the variation in the entropy is constant. On the other hand, the variation of the mean energy increases linearly with w_L, being higher for $w_L < 0$ than for $w_L > 0$.

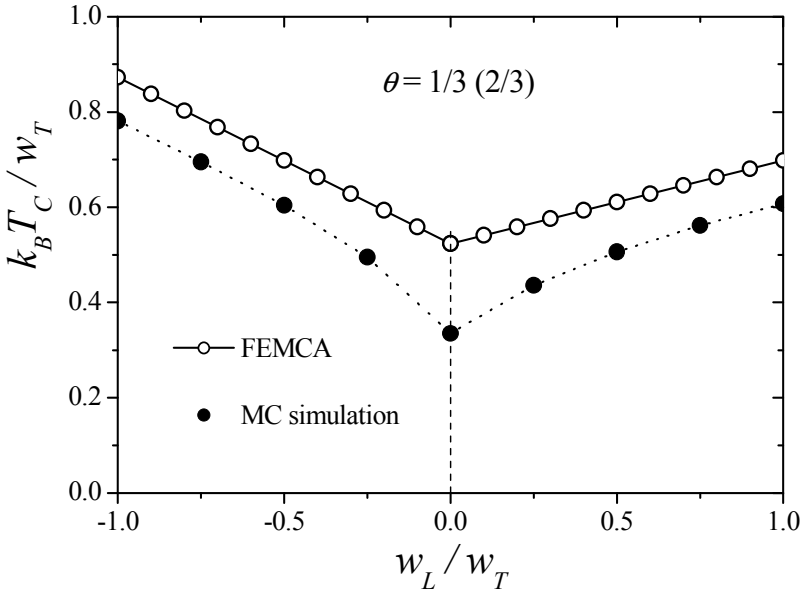

Fig. 22 Comparison between simulated and theoretical results for $k_B T_c / w_T$ vs w_L / w_T at □□=1/3 (2/3).
The dotted lines are a guide for the eyes.

Summary

In the present work, we have addressed the critical properties of a simple lattice-gas model, which mimics a nanoporous environment, where each channel or unit cell is represented by a one-dimensional array. The results were obtained by using MC simulations, finite-size scaling theory and the recently reported FEMCA, which is based on a free energy minimization criterion.

The system was characterized by two parameters w_L/w_T and k_BT/w_T, being w_L and w_T, the longitudinal and transverse energies, respectively. We focused on the case of repulsive transverse interaction energy among adsorbed particles (wT=1) and θ =1/3(2/3), in such a way that a rich variety of ordered phases are observed in the adlayer.

1) For w_L / w_T=0, the system is equivalent to the well-known triangular lattice in 2D.

2) For $w_L / w_T < 0$, the formation of pairs of nearest-neighbor adsorbed particles along the lines is favored. Consequently, the $(\sqrt{3}\times\sqrt{3})$ and $(\sqrt{3}\times\sqrt{3})^*$ phases are reinforced and extend along the

channels. The critical temperature decreases from 0.7817(1) for $w_L/w_T = -1$ to 0.3354(1) for $w_L/w_T=0$.

3) For $w_L/w_T > 0$, the $(\sqrt{3}\times\sqrt{3})$ and $(\sqrt{3}\times\sqrt{3})^*$ structures are formed in the planes at low temperatures and order along the channels in an array of alternating particles. The critical temperature increases from 0.3354(1) for $w_L/w_T=0$ to 0.6098(5) for $w_L/w_T=1$.

With respect to the analytical approach, FEMCA provides results in very good qualitative agreement with MC simulations and constitutes a theoretical framework in order to interpret the behavior of k_BT_c/w_T vs w_L/w_T in the critical concentrations.

Acknowledgments

This work was supported in part by CONICET (Argentina) under project PIP 6294; Universidad Nacional de San Luis (Argentina) under project 322000 and the National Agency of Scientific and Technological Promotion (Argentina) under project 33328 PICT.

References

[1] T.L. Hill: *An Introduction to Statistical Thermodynamics* (Addison-Wesley, Reading, MA, 1960).

[2] H.E. Stanley: *Introduction to Phase Transitions and Critical Phenomena* (Oxford University Press, New York, 1971).

[3] I. Langmuir: J. Am. Chem. Soc. Vol. 34 (1912), 1310; I. Langmuir: J. Am. Chem. Soc. Vol. 37, (1951), p. 417; I. Langmuir: J. Am. Chem. Soc. Vol. 54 (1932), p. 2798; I. Langmuir: Gen. Electr. Rev. Vol. 29 (1926), p. 153; I. Langmuir and K.H. Kingdom: Proc. R. Soc. London, Ser. A Vol. 107 (1925), p. 61; I. Langmuir and K.H. Kingdom: Phys. Rev. Vol. 34 (1919), p. 129; I. Langmuir and J.B. Taylor: Phys. Rev. Vol. 44 (1933), p. 423; I. Langmuir and D.S. Villars: J. Am. Chem. Soc. Vol. 53 (1931), p. 486

[4] E. Ising, Z. Phys. Vol. 31 (1925), p. 253

[5] H.A. Kramers and G.H. Wannier: Phys. Rev. Vol. 60 (1941), p. 252; H.A. Kramers and G.H. Wannier: Phys. Rev. Vol. 60 (1941), p. 263

[6] E. Montroll: J. Chem. Phys. Vol. 9 (1941), p. 706

[7] L. Onsager: Phys. Rev. Vol. 65 (1944), p. 117

[8] K. Binder and D.P. Landau: Phys. Rev. B Vol. 21 (1980), p. 1941

[9] A.J. Ramirez-Pastor, F. Bulnes and G. Zgrablich: Surf. Sci. Vol. 536 (2003), p. 97

[10] A.J. Phares and F.J. Wunderlich: J. Math. Phys. Vol. 26 (1985), p. 2491; A.J. Phares and F.J. Wunderlich: Phys. Rev. E Vol. 52 (1995), p. 2236; A.J. Phares and F.J. Wunderlich: Phys. Rev. E Vol. 55 (1997), p. 2403; A.J. Phares and F.J. Wunderlich: Surf. Sci. Vol. 425 (1999), p. 112; A.J. Phares and F.J. Wunderlich: Surf. Sci. Vol. 452 (2000), p. 108; A.J. Phares and F.J. Wunderlich: Surf. Sci. Vol. 479 (2001), p. 43

[11] F. Romá and A. J. Ramirez-Pastor: Phys. Rev. E Vol. 69 (2004), art. no. 036124

[12] A. Patrykiejew, S. Sokolowski and K. Binder: Surf. Sci. Rep. Vol. 37 (2000), p. 207

[13] F. Bulnes, A.J. Ramirez-Pastor and G. Zgrablich: J. Chem. Phys. Vol. 115 (2001), p. 1513; F. Bulnes, A.J. Ramirez-Pastor and G. Zgrablich: Phys. Rev. E Vol. 65 (2002), art. no. 31603

[14] T. Nitta, M. Kuro-Oka and K. Katayama: J. Chem. Eng. Jpn. Vol. 17 (1984), p. 45

[15] W. Rudzinski, K. Nieszporek, J.M. Cases, L.I. Michot and F. Villeras: Langmuir Vol. 12 (1996), p. 170

[16] M. Borówko and W. Rżysko: J. Colloid Interface Sci. Vol. 182 (1996), p. 268; M. Borówko and W. Rżysko: Ber. Bunsenges. Phys. Chem. Vol. 101 (1997), p. 84

[17] W. Rżysko and M. Borówko: J. Chem. Phys. Vol. 117 (2002), p. 4562; W. Rżysko and M. Borówko: Surf. Sci. Vol. 520 (2002), p. 151

[18] A.J. Ramirez-Pastor, T.P. Eggarter, V.D. Pereyra and J. L. Riccardo: Phys. Rev. B 59 (1999), p. 11027

[19] A.J. Ramirez-Pastor, J.L. Riccardo and V.D. Pereyra: Surf. Sci. Vol. 411 (1998), p. 294; A.J. Ramirez-Pastor, J.L. Riccardo and V.D. Pereyra: Langmuir Vol. 16 (2000), p. 10169

[20] F. Romá, A.J. Ramirez-Pastor and J.L. Riccardo: Langmuir Vol. 16 (2000), p. 9406; F. Romá, A.J. Ramirez-Pastor and J.L. Riccardo: J. Chem. Phys. Vol. 114 (2001), p. 10932

[21] F. Romá, A.J. Ramirez-Pastor and J.L. Riccardo: Phys. Rev. B Vol. 68 (2003), art. no. 205407

[22] S. Iijima: Nature Vol. 354 (1991), p. 56

[23] S. Iijima and T. Ichihashi: Nature Vol. 363 (1993), p. 603

[24] D.S. Bethune, C.H. Kiamg, M.S. deVries, G. Gorman, R. Savoy, J. Vasquez and R. Beyers: Nature Vol. 363 (1993), p. 605

[25] P.M. Ajayan and S. Iijima: Nature Vol. 361 (1993), p. 333

[26] E. Dujardin, T.W. Ebbesen, H. Hiura and K. Tanigaki: Science Vol. 265 (1994), p. 1850

[27] C. Martin, J. P. Coulomb, Y. Grillet and R. Kahn, in: *Fundamentals of Adsorption: Proceedings of the Fifth International Conference*, edited by M.D. LeVan, Kluwer Academic, Boston, MA (1996).

[28] C. Martin, N. Tosi-Pellenq, J. Patarin and J.P. Coulomb: Langmuir Vol. 14 (1998), p. 1774

[29] A.D. Migone and S. Talapatra, in: *Encyclopedia of Nanoscience and Nanotechnology*, edited by H.S. Nalwa, American Scientific, Los Angeles, CA (2004).

[30] G. Stan, M.J. Bojan, S. Curtarolo, S.M. Gatica and M.W. Cole: Phys. Rev. B Vol. 62 (2000), p. 2173

[31] T. Wilson, A. Tyburski, M.R. DePies, O.E. Vilches, D. Becquet and M. Bienfait: J. Low Temp. Phys. Vol. 126 (2002), p. 403

[32] T. Wilson and O.E. Vilches: Low Temp. Phys. Vol. 29 (2003), p 732.

[33] N. M. Urban, S.M. Gatica, M. W. Cole and J. L. Riccardo: Phys. Rev. B Vol. 71 (2005), art. no. 245410

[34] M. Bienfait, P. Zeppenfeld, N. Dupont-Pavlovsky, M. Muris, M.R. Johnson, T. Wilson, M. DePies and O. E. Vilches: Phys. Rev. B Vol. 70 (2004), art. no. 035410

[35] M.M. Calbi, S.M. Gatica, M.J. Bojan, G. Stan and M.W. Cole: Rev. Mod. Phys. Vol. 73 (2001), p. 857

[36] M.M. Calbi and J.L. Riccardo: Phys. Rev. Lett. Vol. 94 (2005), art. no. 246103

[37] R.A. Trasca, M.M. Calbi and M.W. Cole: Phys. Rev. E Vol. 65 (2002), art. no. 061607

[38] R.A. Trasca, M.M. Calbi, M.W. Cole and J.L. Riccardo: Phys. Rev. E Vol. 69 (2004), art. no. 011605

[39] L. Chen and J.K. Johnson: Phys. Rev. Lett. Vol. 94 (2005), art. no. 125701

[40] J.V. Pearce, M.A. Adams, O.E. Vilches, M.R. Johnson and H.R. Glyde, Phys. Rev. Lett. Vol. 95 (2005), art. no. 185302

[41] L. Heroux, V. Krungleviciute, M.M. Calbi and A.D. Migone: J. Phys. Chem. B Vol. 110 (2006), p. 1297

[42] S.M. Gatica, M.J. Bojan, G. Stan and M.W. Cole: J. Chem. Phys. Vol. 114 (2001), p. 3765

[43] W. Shi and K.J. Johnson: Phys. Rev. Lett. Vol. 91 (2003), art. no. 015504

[44] A. Kuznetsova, J.T. Yates, Jr., J. Liu and R.E. Smalley: J. Chem. Phys. Vol. 112 (2000), p. 9590

[45] A. Kuznetsova, D.B. Mawhinney, V. Naumenko, J.T. Yates, Jr.,J. Liu and R.E. Smalley: Chem. Phys. Lett. Vol. 321 (2000), p. 292

[46] M.W. Cole, V.H. Crespi, G. Stan, C. Ebner, J.M. Hartman, S. Moroni and M. Boninsegni: Phys. Rev. Lett. Vol. 84 (2000), p. 3883

[47] G.F. Newell and E.W. Montroll: Rev. Mod. Phys. Vol. 25 (1953), p. 353

[48] M. Schick, J.S. Walker and M. Wortis, Phys. Lett. Vol. 58 (1976), p. 479

[49] M. Schick, J.S. Walker and M. Wortis: Phys. Rev. B Vol. 16 (1977), p. 2205

[50] C.E. Campbell and M. Schick: Phys. Rev. A Vol. 5 (1972), p. 1919

[51] A.N. Berker, S. Ostlund and F.A. Putnam: Phys. Rev. B Vol. 17 (1978), p. 3650

[52] R.B. Griffiths: Phys. Rev. Vol. 136 (1964), p. A437

[53] R.B. Griffiths: J. Math. Phys. Vol. 8 (1967), p. 478; R.B. Griffiths: J. Chem. Phys. Vol. 8 (1967), p. 484

[54] C.-Y. Weng, R.B. Griffiths and M.E. Fisher: Phys. Rev. Vol. 162 (1967), p. 475

[55] M.E. Fisher: Phys. Rev. Vol. 162 (1967), p. 480

[56] P.M. Pasinetti, J.L. Riccardo and A.J. Ramirez-Pastor: J. Chem. Phys. Vol. 122 (2005) art. no. 154708

[57] P.M. Pasinetti, J.L. Riccardo and A.J. Ramirez-Pastor: Physica A Vol. 355 (2005), p. 383

[58] P.M. Pasinetti, F. Romá, J. L. Riccardo, and A. J. Ramirez-Pastor, J. Chem. Phys. Vol. 125 (2006), art. no. 214705

[59] D. Nicholson and N.G. Parsonage: *Computer Simulation and the Statistical Mechanics of Adsorption* (Academic Press, London 1982).

[60] N. Metropolis, A.W. Rosenbluth, M.N. Rosenbluth, A.H. Teller and E. Teller: J. Chem. Phys. Vol. 21 (1953), p. 1087

[61] V.A. Bakaev and W.A. Steele: Langmuir Vol. 9 (1992), p. 148

[62] A.J. Ramirez-Pastor and F. Bulnes: Physica A Vol. 283 (2000), p. 198

[63] F. Bulnes and A.J. Ramirez-Pastor: Physica A Vol. 295 (2001), p. 71

[64] K. Hukushima and K. Nemoto: J. Phys. Soc. Jpn. Vol, 65 1604 (1996).

[65] D.J. Earl and M.W. Deem: Phys. Chem. Chem. Phys. Vol. 7 (2005), p. 3910

[66] K. Binder: *Applications of the Monte Carlo Method in Statistical Physics: Topics in Current Physics* (Springer, Berlin 1984).

[67] M.E. Fisher, in: *Critical Phenomena*, edited by M.S. Green (Academic, London 1971).

[68] V. Privman: *Finite Size Scaling and Numerical Simulation of Statistical Systems* (World Scientific, Singapore 1990).

[69] M.R. Swift, E. Cheng, M. W. Cole and J. R. Banavar: Phys. Rev. B Vol. 48 (1993), p. 3124

[70] R. Radhakrishnan and K. E. Gubbins: Phys. Rev. Lett. 79 (1997), p. 2847

[71] D.P. Landau: Phys. Rev. B Vol. 27 (1983), p. 5604

[72] A.A. Tarasenko, F. Nieto, L. Jastrabík and C. Uebing: Phys. Rev. B Vol. 64 (2001) art. no. 075413

[73] P. M. Pasinetti, F. Romá, J. L. Riccardo, and A. J. Ramirez-Pastor: Phys. Rev. B Vol. 74 (2006), art. no. 155418

[74] B.D. Metcalf: Phys. Lett. A Vol. 45 (1973), p. 1

[75] W. Kinzel and M. Schick: Phys. Rev. B Vol. 23 (1981), p. 3435

[76] K.K. Chin and D.P. Landau: Phys. Rev. B Vol. 36 (1987), p. 275

[77] E. Barouch, B.M. McCoy and T.T. Wu: Phys. Rev. Lett. Vol. 31 (1973), p. 1409

[78] K. Binder and J.S. Wang: J. Stat. Phys. Vol. 55 (1989), p. 87